Rapid Assembly of Heterogeneous 3D Cell Microenvironments in a Microgel Array

*Yiwei Li, Pu Chen, Yachao Wang, Shuangqian Yan, Xiaojun Feng, Wei Du, Stephan A. Koehler, Utkan Demirci, and Bi-Feng Liu**

Cells in biological tissues are living in a highly complex 3D local microenvironment comprising spatially heterogeneous chemical cues, extracellular matrix, and cell populations.[1–5] Generating heterogeneous 3D cell microenvironment arrays in vitro with controlled and spatially organized components over individual microenvironments is urgently demanded in emerging fields such as stem cell research, personalized in vitro disease model, and microscale tissue engineering.[6–15] Bioengineering of single 3D complex cell microenvironment has been previously demonstrated using various approaches, including microrobotics,[16] microfluidics,[17–19] electrostatics,[20] acoustics,[21–23] magnetics,[24,25] and photolithography.[6,26] However, few of these approaches enable effective formation of heterogeneous 3D cell microenvironment arrays.[27–29] Robotic liquid-dispensing systems are widely used to create 3D cell-encapsulating biomaterial microarrays, but these systems do not have control over spatial distribution of different components in individual biomaterial spots.[27,28,30–32] Furthermore, these systems are generally designed for industrial customers and are not cost-effective for biomedical/biological labs that need a simple, cost-effective solution for high-throughput screening (HST).[33–35] Surface wettability techniques have been long utilized to create microdroplet arrays and microgel arrays for various applications such as condensation of water, stem cell research, cell patterning, and cell-based HST.[35–40] However, generation of spatially controlled heterogeneous 3D microenvironment arrays has not been presented.

Herein, we present a simple and cost-effective method to rapidly assemble heterogeneous 3D cell microenvironment in microgel arrays by combining surface-wettability-guided assembly (SWGA) and microdroplet-array-based operations. To create wettability micropatterned surface for SWGS, we uniquely explore a simple surface modification method based on a widely accessible polydimethylsiloxane (PDMS) stamping approach (**Figure 1**). Briefly, we fabricate a PDMS stamp with a desired micropattern using conventional soft lithography.[41] The PDMS stamp and a clean glass slide are treated with oxygen plasma and temporarily bonded together. After detaching the PDMS stamp from the glass slide, the glass regions in contact with the PDMS surface were coated with a nanofilm of PDMS oligomers, which are visible using a scanning electron microscope (SEM) (Figure 1b, Figure S1, and "Fabrication of wettability-patterned surface" in the Supporting Information). The PDMS nanofilm is hydrophobic with a water contact angle of 125°, whereas that of the glass slide without the nanofilm is 27° (Figure 1c and "Measurement of water contact angle" in the Supporting Information). The hydrophobic/hydrophilic contact line at the PDMS-glass interface provides a pinned boundary condition for stabilizing sessile microdroplets in hydrophilic regions. Attenuated total reflectance Fourier-transform infrared spectroscopy (ATR-FTIR) absorption spectra show the PDMS nanofilm has methyl groups, which are hydrophobic, whereas the glass surface has hydroxyl groups, which are hydrophilic (Figure 1d, Table S1, "ATR-FTIR measurement," and Figure S2 in the Supporting Information). This wettability micropattern causes wetting of aqueous solutions to hydrophilic regions and repulsion of aqueous solutions from hydrophobic regions. By spreading a hydrogel prepolymer on the wettability-patterned surface, a microdroplet array self-assembles within a few seconds and is transformed into a microgel array via gelation (Figure 1a and Movie S1 in the Supporting Information).

Our technique can be used to fabricate microgel arrays with individual microgels sized from 2 mm down to 20 μm (Figure S3, Supporting Information), corresponding to microgel density from a few microgels per square centimeter to one hundred thousand microgels per square centimeter. The thickness of microgels depends on the contact angle and microgel diameter. We illustrate very uniform, highly repeatable microgel arrays with microgel sizes from 100 to 800 μm (Figure 1e,f) which are corresponding to the microgel thickness from 5 to 45 μm (Figure S4, Supporting Information). The self-assembled microgels have a very small variation in their sizes, which is indicated by quantitative fluorescence

Y. W. Li, Y. C. Wang, S. Q. Yan, Prof. X. J. Feng, Prof. W. Du, Prof. B.-F. Liu
Britton Chance Center for Biomedical Photonics at Wuhan National Laboratory for Optoelectronics – Hubei Bioinformatics & Molecular Imaging Key Laboratory
Systems Biology Theme
Department of Biomedical Engineering
College of Life Science and Technology
Huazhong University of Science and Technology
Wuhan 430074, P. R. China
E-mail: bfliu@mail.hust.edu.cn

Y. W. Li, Dr. S. A. Koehler
Department of Applied Physics
John A. Paulson School of Engineering and Applied Sciences
Harvard University
Cambridge, MA 02138, USA

Dr. P. Chen, Prof. U. Demirci
Department of Radiology
School of Medicine
Stanford University
Palo Alto, CA 94304, USA

DOI: 10.1002/adma.201600247

ADVANCED MATERIALS
www.advmat.de

www.MaterialsViews.com

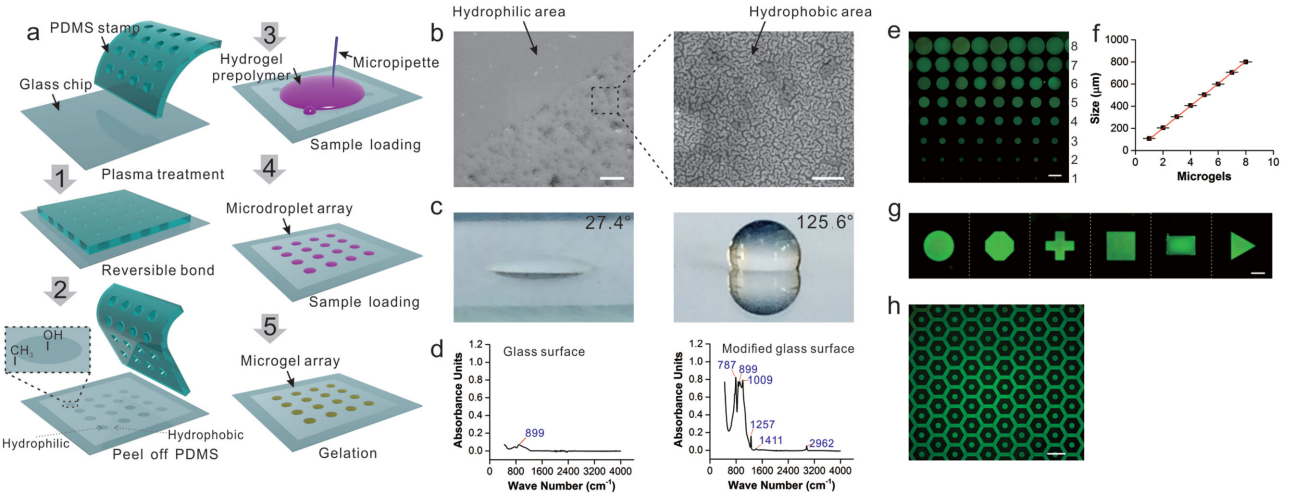

Figure 1. Surface-wettability-guided assembly of microgel arrays. a) Schematics of wettability-guided assembly of a microgel array. b) SEM of PDMS nanofilm. Scale bar, 4 μm in the left image, 500 nm in the right image. c) Water-contact-angle measurements for plasma-treated glass and PDMS nanofilm; d) ATR-FTIR analysis of unmodified glass and PDMS-nanofilm-stamped glass. e) Assembly of size-varied PEG microgels. Scale bar, 600 μm. f) Quantitative analysis of size variation of assembled microgels. The data represent mean ± standard deviation (SD) ($n = 10$). g) Assembly of shape-varied PEG-microgel arrays. Scale bar, 300 μm. h) Assembly of a complex PEG-hydrogel architecture. Scale bar, 600 μm.

analysis (Figure S5 and S6, Supporting Information). Using this method, we fabricate microgels with varied geometries, including circles, squares, octagons, crosses, triangles, as well as complex interconnected microgel networks (Figure 1g).

We demonstrate assembly of microgel arrays with spatially defined multiple components, which is essential for investigation of complex cell–cell and cell–ECM (extracellular matrix) interactions in local microenvironments (**Figure 2**). Cell-encapsulating microgel arrays were generated with spatially organized heterogeneous cell populations over individual microgels. In the first approach, we explore layer-by-layer assembly of two cell types (Figure 2a). A microgel array containing Human Umbilical Vein Endothelial Cells (HUVECs) is first prepared as described above and then immersed in hydrogel prepolymer containing fibroblast cells. After withdrawing extra solution, hydrogel prepolymer is self-assembled on the top of the generated microgels due to hydrophilic property of microgels. After gelation, two-layered microgel arrays (Figure 2b) are obtained with one layer of HUVECs stacked with one layer of fibroblast cells, confirmed by confocal florescence imaging (Figure 2c–e). In another approach, we explore fusion of two microdroplets side by side for formation of the compartmented heterogeneous cell populations (Figure 2f). Cell-encapsulating microdroplet array is first made with pairs of microdroplets containing either HUVECs or fibroblasts (Figure 2g), which was prepared by dispensing prepolymer solution containing suspended HUVECs or fibroblast on a column of hydrophilic regions using a micropipetting system (Note S1 in the Supporting Information). The microdroplet pair is then fused into a large microdroplet on another glass slide at the bottom. After cells sediment to the bottom of the fused droplet, the top glass slide previously containing microdroplet pairs was departed from the bottom glass slide containing large microdroplets (Figure 2h). After gelation, HUVECs and fibroblasts are encapsulated in individual microgels in a side-by-side spatial organization (Figure 2i). The assembled cell co-culture system can be used as an in vitro model to study fibroblast-endothelial cell interactions and angiogenesis under a given heterogeneous cell organization. To evaluate cytocompatibility of this SWGA, we characterize cell viability and proliferation using LIVE/DEAD Assays and immunostaining of anti-Ki67 marker, respectively. The viability assay indicates more than 90% live cells (Figure S7a–c, Supporting Information), and the Ki67 index further shows more than 50% cell nuclear proliferation over 4 d in the 3D tissue culture (Figure S7d–f and Note S2 in the Supporting Information).

In addition, these heterogeneous microgel arrays can be easily integrated into a 3D hydrogel sheet to form a spatially defined chemical, cell, and/or biomaterial distribution (Figure 2j). As an example, an agarose microgel array containing 500×10^{-9} M fluorescein was self-assembled as described above. Surface wettability of PDMS nanofilm around agarose microgels was converted into hydrophilic via treatment of methacrylatesilane, which contains double bonds allowing hydrophilic polymers grafted to the surface. Hydrophilic PDMS nanofilm was wetted by polyethylene glycol (PEG) prepolymer (10 w/v% poly(ethylene glycol) diacrylate (PEGDA) 1000) containing 500×10^{-9} M rhodamine via capillary effect. After photocrosslinking, we achieved a flat 3D hydrogel sheet, where the first spatially defined microgel array was covered with the secondary hydrogel component (Figure 2k and Movie S2, Supporting Information) as the hydrophilic microgels are wetted by the secondary hydrogel prepolymer solution during solution dispensing. Fluorescence analysis further confirms periodic chemical/biomaterial distribution in the 3D hydrogel sheet (Figure 2l). Additionally, after the formation of 3D hydrogel sheet, fluorescein encapsulated in the agarose gel array slowly diffused into the component PEGDA hydrogel, meanwhile rhodamine encapsulated in the PEGDA gel slowly diffused into the agarose gel array. These 3D hydrogel sheets are potentially useful for investigating cell invasion, cell chemotaxis, and drug release in 3D biomaterials.[10,42,43]

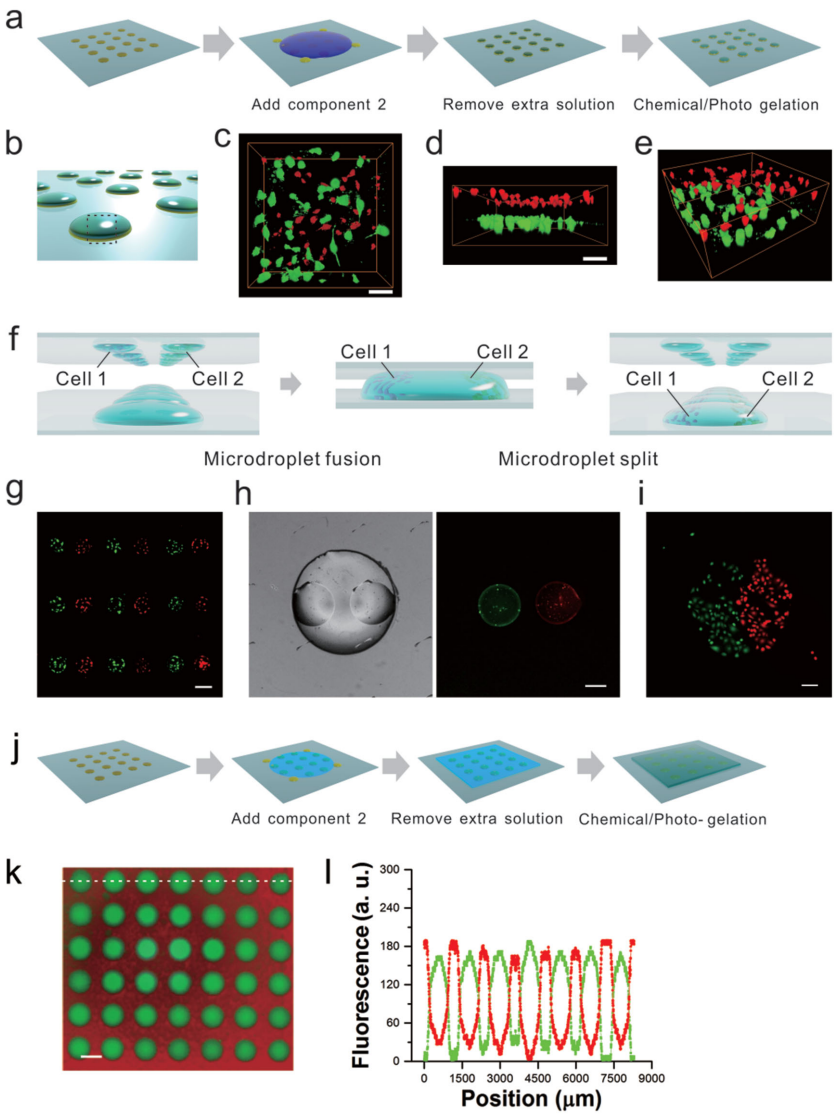

Figure 2. Assembly of microgels with spatially organized multiple components. a) Schematics of layer-by-layer assembly of two cell populations in individual microgels. b) Schematic of bi-layered microgels. c–e) Top-down, side, and perspective views of layer-by-layer assembled cells in a single microgel. Scale bar, 50 μm. f) Schematics of side-by-side assembly of two cell populations in individual microgels. g) Fluorescence image of cell-encapsulating microdroplet array. NIH 3T3 cells were labeled with DiO (green), HUVEC cells were labeled with DiI (red). Scale bar, 300 μm. h) Alignment of paired cell-encapsulating microdroplet with a large microdroplet in both bright-field and fluorescence images. Scale bar, 100 μm. i) Fluorescence image of a single microgel containing side-by-side assembled two cell populations. Scale bar, 100 μm. j) Schematics of assembly of complementary hydrogel structure. k) Agarose hydrogel (green) and PEG hydrogel (red) were assembled into a complementary structure. Scale bar, 800 μm. White dashed line indicates fluorescence analysis in (l). l) Fluorescence analysis of assembled structure at white dashed line in (k). Red and green lines indicate Rhodamine and fluorescein intensity, respectively.

We generate heterogeneous microgel arrays with discrete chemical gradient and cell density gradient over individual microgels (**Figure 3**a). Briefly, one glass slide is prepared with uniform-sized hydrophilic regions while another glass slide is prepared with size-varied hydrophilic regions. The locations of hydrophilic regions on these two glass slides are designed in pairs and corresponding to each other. Two microdroplet arrays are formed by dispensing hydrogel prepolymer with and without a chemical cue on the wettability-micropatterned surfaces, respectively. These two microdroplet arrays are aligned and merged under a CCD camera, and then separated from each other (Figure 3b and Movie S3 in the Supporting Information). The aligned microdroplet pairs are fused and resulted in formation of microgel assays with varying chemical concentration over individual microgels. To avoid lateral fusion between neighboring droplets on the same slide during the alignment, we design the interval between the neighboring droplets to be the half of the large droplet diameter out of the droplet pair with a consideration of the droplet volume change during the vertical droplet fusion (Note S3 in the Supporting Information). The resulting chemical concentrations over individual microgels are related to the volume ratio of merged hydrogel prepolymer droplets (Note S4 in the Supporting Information). We demonstrate this approach by fabricating a uniform circular microgel array (PEGDA 1000, 10 w/v%) with a discrete fluorescein concentration ranging from 30 to 800 × 10^{-9} M with a stepping resolution of around 15 × 10^{-9} M as shown in Figure 3c.

Using the same above approach, we generate a cell-encapsulating microgel array with a cell seeding density ranging from three cells per microgel to 10^2 cells per microgel by merging a size-varied microdroplet array containing 1.5 × 10^6 HUVECs mL^{-1} with a size-uniform microdroplet array without HUVECs (Figure 3d and Note S5 in the Supporting Information). Cells in the hanging size-varied microdroplet array on the top glass slide are transferred to a size-uniform sessile microdroplet array on the bottom glass slide via droplet pairing, fusion, and cell gravitational sediment sequently. After gently separating the top slide from the bottom slide and subsequent gelation, a size-uniform microgel array with a cell density gradient can be achieved on the bottom slide. This microdroplet operation method can also be used to transfer cells between slides from a homogenous cell-encapsulating microdroplet array to another size-uniform blank microdroplet array.

Furthermore, we assemble a complex cell microenvironment array with orthogonal gradients of chemical concentration and cell seeding density for HST. One cell-encapsulating microdroplet array is prepared with a discrete gradient of cell seeding density as described above, while the other microdroplet array is prepared with the same concentration of a chemical cue and varied size over individual microdroplets. By merging these two

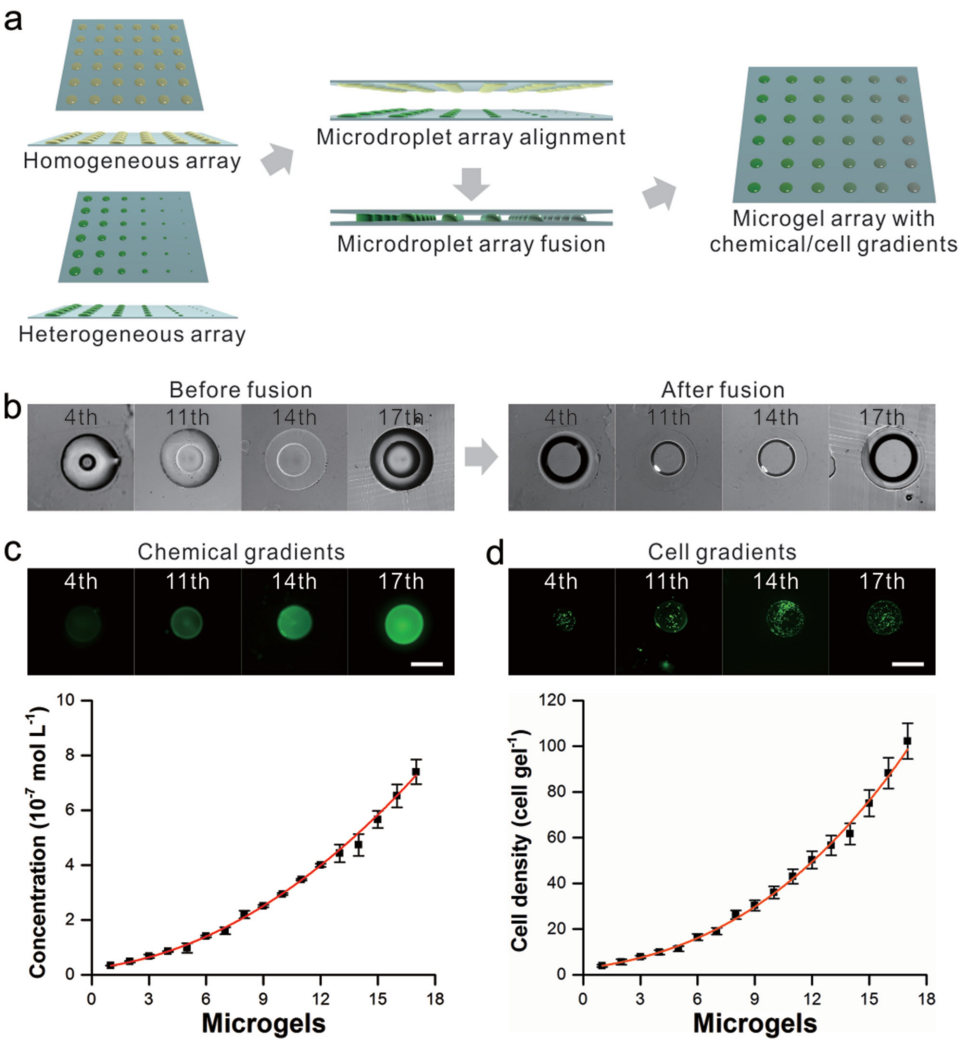

Figure 3. Assembly of heterogeneous microenvironment arrays with chemical/cell gradients. a) Schematics of generation of microgel arrays with chemical/cell gradient using microdroplet-array-based operations. b) Bright-field images of a pair of drops before and after microdroplet fusion. Scale bar, 1 mm. c) Fluorescence images of droplets with chemical gradients and quantitative analysis of chemical concentration. d) Fluorescence images of droplets with cell gradients and quantitative analysis of cell number in individual microgels. Fluorescence images showed the 4th, 11th, 14th, and 17th droplets with increasing concentration from the smallest to the largest. The data represent mean ± SD ($n = 3$).

microdroplet arrays in an orthogonal manner and subsequent photoinitiated gelation, a microgel array is generated containing orthogonal gradients of the chemical concentration and cell seeding density (**Figure 4**a). We generate orthogonal gradients of CdTe quantum dots (QDs) (4-16 × 10^{-9} mol mL^{-1}) and cell seeding density (40–160 HUVECs per microgel) and investigate the nanocytotoxicity of the CdTe QDs on 3D cultured HUVECs. The result shows that cell viability declined with an increase in the QD concentration under varied cell populations (Figure 4b). Correlation analysis further confirms that cell viability is closely correlated with the QD concentration (Figure 4c), which is in good agreement with the concentration-dependent CdTe cytotoxicity in the previous study.[44] Interestingly, cell viability is not linearly correlated with cell seeding density (Figure 4c,d). Cells showed a nonlinear response to QD exposure under QD concentrations of 12 × 10^{-9} mol mL^{-1} and 16 × 10^{-9} mol mL^{-1} and demonstrated a far better survival rate under a seeding density of 80 cells per gel than seeding densities of 40, 120, or 180 cells per gel. In addition, we observed cells appear to be more prone to QD toxicity in 3D comparing with cells in 2D under the same amount of QD concentration.[44–46]

Despite multiple merits such as high throughput, precise control over microenvironment components, and biocompatibility, there are some limitations in our method. All the microdroplet operations (e.g., droplet alignment, fusion, splitting) and liquid dispensing are currently performed manually, which requires practice to achieve good repeatability and controllability. To further improve the repeatability and controllability of this method, the manual operations can be replaced by automatic machines, which can meet the requirements of industrial applications.

In conclusion, we uniquely demonstrate a method that enables rapid assembly of thousands of heterogeneous 3D cell microenvironments with precise control over individual shapes,

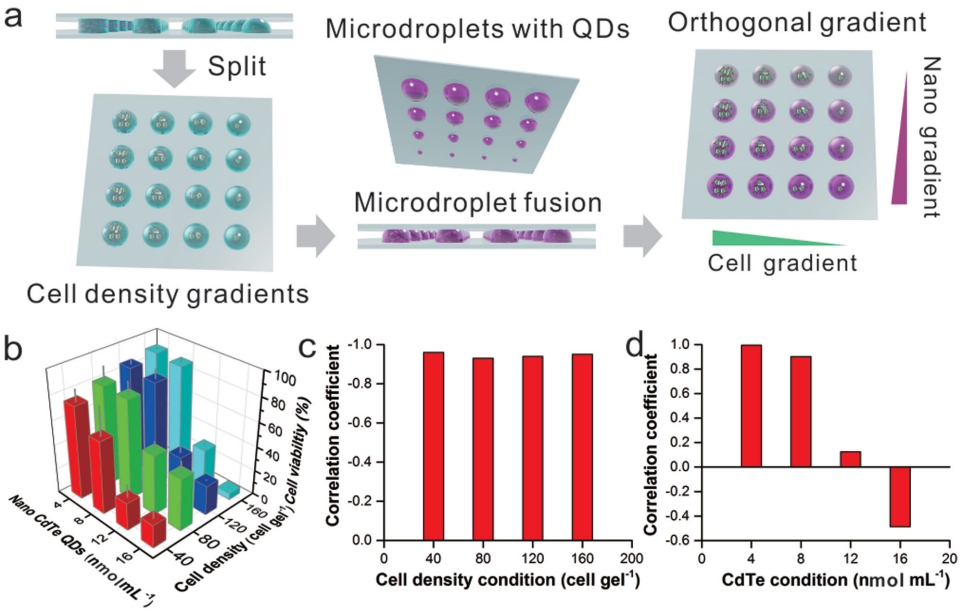

Figure 4. Assembly of complex cell microenvironment arrays with orthogonal gradients. a) Schematics of generation of orthogonal gradients of chemical concentration and cell seeding density over individual microgels. b) Quantitative analysis of nano-CdTe QDs cytotoxicity under varied cell seeding densities and the CdTe QD concentrations. The data represent mean ± SD ($n = 3$). c,d) Correlation analysis of cell viability with the CdTe QDs concentration and cell seeding density.

sizes, chemical concentrations, cell density, and 3D spatial distribution of multiple components. This technique provides a simple and cost-effective solution to meet the increasing demand of creating heterogeneous 3D cell microenvironments for HST in broad fields such as stem cell research, personalized in vitro disease modeling, microscale tissue engineering, and preclinical drug screening.

Supporting Information

Supporting Information is available from the Wiley Online Library or from the author.

Acknowledgements

Y.W.L. and P.C. contributed equally to this work. The authors gratefully acknowledge financial support from the National Natural Science Foundation of China (21475049, 31471257, and 21275060) and the National Basic Research Program of China (2011CB910403).

Received: January 15, 2016
Revised: February 11, 2016
Published online: March 17, 2016

[1] J. A. Joyce, J. W. Pollard, *Nat. Rev. Cancer* **2009**, *9*, 239.
[2] L. Li, T. Xie, *Annu. Rev. Cell Dev. Biol.* **2005**, *21*, 605.
[3] M. Sutherland, K. Fabre, D. Tagle, *Stem Cell Res. Ther.* **2013**, *4*, I1.
[4] C. Bouyer, P. Chen, S. Güven, T. T. Demirtas, T. J. F. Nieland, F. Padilla, U. Demirci, *Adv. Mater.* **2016**, *28*, 161.
[5] W. L. Murphy, T. C. McDevitt, A. J. Engler, *Nat. Mater.* **2014**, *13*, 547.
[6] W. Asghar, H. Shafiee, P. Chen, S. Tasoglu, S. Guven, U. Gurkan, U. Demirci, in *Cancer Targeted Drug Delivery* (Eds: Y. H. Bae, R. J. Mrsny, K. Park), Springer, New York **2013**, p. 635.
[7] D. Huh, G. A. Hamilton, D. E. Ingber, *Trends Cell Biol.* **2011**, *21*, 745.
[8] M. P. Lutolf, J. A. Hubbell, *Nat. Biotechnol.* **2005**, *23*, 47.
[9] E. Santos, R. M. Hernandez, J. L. Pedraz, G. Orive, *Trends Biotechnol.* **2012**, *30*, 331.
[10] Y. Zhang, L. Zhou, L. J. Qin, *J. Am. Chem. Soc.* **2014**, *136*, 15257.
[11] H. Tekin, T. Tsinman, J. G. Sanchez, B. J. Jones, G. Camci-Unal, J. W. Nichol, R. Langer, A. Khademhosseini, *J. Am. Chem. Soc.* **2011**, *133*, 12944.
[12] N. Annabi, A. Tamayol, J. A. Uquillas, M. Akbari, L. E. Bertassoni, C. Cha, G. Camci-Unal, M. R. Dokmeci, N. A. Peppas, A. Khademhosseini, *Adv. Mater.* **2014**, *26*, 85.
[13] D. W. Hutmacher, D. Loessner, S. Rizzi, D. L. Kaplan, D. J. Mooney, J. A. Clements, *Trends Biotechnol.* **2010**, *28*, 125.
[14] B. E. Uygun, A. Soto-Gutierrez, H. Yagi, M.-L. Izamis, M. A. Guzzardi, C. Shulman, J. Milwid, N. Kobayashi, A. Tilles, F. Berthiaume, *Nat. Med.* **2010**, *16*, 814.
[15] E. Jabbari, *Curr. Opin. Biotechnol.* **2011**, *22*, 655.
[16] S. Tasoglu, E. Diller, S. Guven, M. Sitti, U. Demirci, *Nat. Commun.* **2014**, *5*, 3124.
[17] E. Kang, G. S. Jeong, Y. Y. Choi, K. H. Lee, A. Khademhosseini, S.-H. Lee, *Nat. Mater.* **2011**, *10*, 877.
[18] S. Sant, M. J. Hancock, J. P. Donnelly, D. Iyer, A. Khademhosseini, *Can. J. Chem. Eng.* **2010**, *88*, 899.
[19] T. Rossow, J. A. Heyman, A. J. Ehrlicher, A. Langhoff, D. A. Weitz, R. Haag, S. Seiffert, *J. Am. Chem. Soc.* **2012**, *134*, 4983.
[20] Y. L. Han, Y. Yang, S. Liu, J. Wu, Y. Chen, T. J. Lu, F. Xu, *Biofabrication* **2013**, *5*, 035004.
[21] P. Chen, S. Guven, O. B. Usta, M. L. Yarmush, U. Demirci, *Adv. Healthcare Mater.* **2015**, *4*, 1937.
[22] P. Chen, Z. Luo, S. Guven, S. Tasoglu, A. V. Ganesan, A. Weng, U. Demirci, *Adv. Mater.* **2014**, *26*, 5936.
[23] F. Xu, T. D. Finley, M. Turkaydin, Y. Sung, U. A. Gurkan, A. S. Yavuz, R. O. Guldiken, U. Demirci, *Biomaterials* **2011**, *32*, 7847.

[24] S. Tasoglu, D. Kavaz, U. A. Gurkan, S. Guven, P. Chen, R. Zheng, U. Demirci, *Adv. Mater.* **2013**, *25*, 1137.
[25] F. Xu, C.-M. Wu, V. Rengarajan, T. D. Finley, H. O. Keles, Y. Sung, B. Li, U. A. Gurkan, U. Demirci, *Adv. Mater.* **2011**, *23*, 4254.
[26] Y. K. Cheung, E. U. Azeloglu, D. A. Shiovitz, K. D. Costa, D. Seliktar, S. K. Sia, *Angew. Chem. Int. Ed.* **2009**, *48*, 7188.
[27] D. G. Anderson, S. Levenberg, R. Langer, *Nat. Biotechnol.* **2004**, *22*, 863.
[28] D. G. Anderson, D. Putnam, E. B. Lavik, T. A. Mahmood, R. Langer, *Biomaterials* **2005**, *26*, 4892.
[29] S. Zhao, H. Zhao, X. Zhang, Y. Li, Y. Du, *Lab Chip* **2013**, *13*, 2350.
[30] T. G. Fernandes, M. M. Diogo, D. S. Clark, J. S. Dordick, J. M. Cabral, *Trends Biotechnol.* **2009**, *27*, 342.
[31] X. Li, X. Zhang, S. Zhao, J. Wang, G. Liu, Y. Du, *Lab Chip* **2014**, *14*, 471.
[32] A. Ranga, S. Gobaa, Y. Okawa, K. Mosiewicz, A. Negro, M. P. Lutolf, *Nat. Commun.* **2014**, *5*, 4324.
[33] T. Billiet, M. Vandenhaute, J. Schelfhout, S. Van Vlierberghe, P. Dubruel, *Biomaterials* **2012**, *33*, 6020.
[34] V. Mironov, R. P. Visconti, V. Kasyanov, G. Forgacs, C. J. Drake, R. R. Markwald, *Biomaterials* **2009**, *30*, 2164.
[35] A. A. Popova, S. M. Schillo, K. Demir, E. Ueda, A. Nesterov-Mueller, P. A. Levkin, *Adv. Mater.* **2015**, *27*, 5217.
[36] I. Orkan Ucar, H. Y. Erbil, *Turk. J. Chem.* **2013**, *37*, 643.
[37] E. Ueda, F. L. Geyer, V. Nedashkivska, P. A. Levkin, *Lab Chip* **2012**, *12*, 5218.
[38] E. Ueda, P. A. Levkin, *Adv. Mater.* **2013**, *25*, 1234.
[39] B. Su, Y. Tian, L. Jiang, *J. Am. Chem. Soc.* **2016**, *138*, 1727.
[40] N. N. T. Le, S. Zorn, S. K. Schmitt, P. Gopalan, W. L. Murphy, *Acta Biomater.* **2015**, DOI: 10.1016/j.actbio.2015.09.019.
[41] Y. Li, X. Feng, Y. Wang, W. Du, P. Chen, C. Liu, B. F. Liu, *Lab Chip* **2015**, *15*, 3203.
[42] K. Vulic, M. S. Shoichet, *J. Am. Chem. Soc.* **2012**, *134*, 882.
[43] H. Tekin, T. Tsinman, J. G. Sanchez, B. J. Jones, G. Camci-Unal, J. W. Nichol, R. Langer, A. Khademhosseini, *J. Am. Chem. Soc.* **2011**, *133*, 12944.
[44] J. Lovri , S. J. Cho, F. M. Winnik, D. Maysinger, *Chem. Biol.* **2005**, *12*, 1227.
[45] J. Lovric, H. S. Bazzi, Y. Cuie, G. R. A. Fortin, F. M. Winnik, D. J. Maysinger, *Mol. Med.—JMM* **2005**, *83*, 377.
[46] J. Lovric, S. J. Cho, F. M. Winnik, D. Maysinger, *Chem. Biol.* **2005**, *12*, 1227.